Inorganic Chemistry

pubs.acs.org/IC Article

Hydrogen Bonding Propagated Phase Separation in Quasi-Epitaxial Single Crystals: A Pd−Br Molecular Insulator

Takefumi Yoshida,* Shinya Takaishi,* Laurent Guérin, Tatsuhiro Kojima, Hiroyoshi Ohtsu, Masaki Kawano, Tatsuya Miyamoto, Hiroshi Okamoto, Kenichi Kato, Masaki Takata, Yuka Hosomi, Shoji Yoshida, Hidemi Shigekawa, Hisaaki Tanaka, Shin-ichi Kuroda, Hiroaki Iguchi, Brian K. Breedlove, Zhao-Yang Li, and Masahiro Yamashita*

Cite This: *Inorg. Chem.* 2022, 61, 14067−14074 Read Online

ACCESS | Metrics & More | Article Recommendations | Supporting Information

ABSTRACT: In condensed matter, phase separation is strongly related to ferroelasticity, ferroelectricity, ferromagnetism, electron correlation, and crystallography. These ferroics are important for nano-electronic devices such as non-volatile memory. However, the quantitative information regarding the lattice (atomic) structure at the border of phase separation is unclear in many cases. Thus, to design electronic devices at the molecular level, a quantitative electron−lattice relationship must be established. Herein, we elucidated a Pd^{II}−Pd^{IV}/Pd^{III}−Pd^{III} phase transition and phase separation mechanism for $[Pd(cptn)_2Br]Br_2$ (cptn = 1*R*,2*R*-diaminocyclopentane), propagated through a hydrogen-bonding network. Although the Pd···Pd distance was used to determine the electronic state, the differences in the Pd···Pd distance and the optical gap between Mott−Hubbard (MH) and charge-density-wave (CDW) states were only 0.012 Å and 0.17 eV, respectively. The N−H···Br···H−N hydrogen-bonding network functioned as a jack, adjusting the structural difference dynamically, and allowing visible ferroelastic phase transition/separation in a fluctuating N_2 gas flow. Additionally, the effect of the phase separation on the spin susceptibility and electrical conductivity were clarified to represent the quasi-epitaxial crystals among CDW−MH states. These results indicate that the phase transitions and separations could be controlled via atomic and molecular level modifications, such as the addition of hydrogen bonding.

INTRODUCTION

Phase separation in condensed matter, where multiple phases/domains coexist in a single component, is intrinsically linked to ferroelasticity, ferroelectricity, ferromagnetism, electron-correlation, and crystallography.[1−13] Significantly, the compound maintains several ferroelastic domains due to spontaneous strain, which is induced by a chemical bond or an interaction against the lattice strain that occurs during the phase transition. In particular, physical properties have a direct effect on the states at the interfaces between the phases. In addition, external stimuli can be used to control some of the domains of ferroics or multiferroics.[3,4] As a result, scientists have created numerous compounds and analyzed the interfaces using a variety of techniques.[1−13]

Phase separation has been widely reported for metal oxides, and it is frequently accompanied by ferroelasticity and ferroelectricity.[5,6] Wei et al. have reported that the phase separation in ferroelectric $Pb(Zr_{0.1}Ti_{0.9})O_3$ thin films can be controlled by modifying the domain wall bending, type of doping, polarization orientation, and the work functions of adjacent electrodes.[5] At the atomic scale, the ferroelastic domains (walls) of oxides have been observed using a transmission electron microscope (TEM). Some oxides exhibit micrometer-scale phase separation.[7]

Although phase separations in organic molecular solids are relatively rare in comparison to metal oxides, Takamizawa et al. have reported superelastic organic molecules.[8,9] A single crystal of 1,3-bis(4-methoxyphenyl)urea has been reported to demonstrate both superelasticity and ferroelasticity via single-crystal-to-single-crystal twinning.[8] However, crystallographic boundaries with a significant NH···O hydrogen-bonding network occur.[8] Thus, there has been a surge of interest in elastic phase separation over the last several years.

Tetracyanoquinodimethane (TCNQ)[10,11] and bis(ethylenedithio)tetrathiafulvalene (BEDT-TTF)[12,13] salts have been used to demonstrate phase separation in organic semiconductors via charge-transfer phase transitions (CTPTs). Kumai et al. have reported a current-induced insulator−metal transition in K-TCNQ,[10] where the dimerized and partially dimerized domains form an alternate phase separation along the π stacks due to lattice strain.[11] Moreover, Pustogow et al. have observed a metal-to-insulator transition for α-$(BEDT\text{-}TTF)_2I_3$ using cryogenic scanning near-field optical microscopy, and they report that the phase transition and phase

Received: June 15, 2022
Published: August 25, 2022

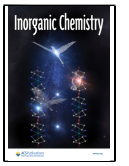

https://doi.org/10.1021/acs.inorgchem.2c02078
Inorg. Chem. 2022, 61, 14067−14074

separation were caused by the internal strain distribution in the crystal.[13] Despite the strong correlation between the lattice and the electrons, α-(BEDT-TTF)$_2$I$_3$ has no crystallographic phase boundaries.[12,13] Although structural and orientational information has been reported, studies offering quantitative lattice (atomic) information have been limited. Thus, for the molecular design of the electronic devices, a quantitative relationship between the lattice and the electrons should be established.[1−3]

Quasi-one-dimensional halogen-bridged metal (MX) complexes are excellent candidates for deciphering CTPT lattice−electron correlations.[14−16] The MX chain comprises an isolated one-dimensional (1D) electronic system composed of the dz^2 orbital of metal ions (M) and the pz orbital of bridging halide ions (X),[16] and an extended Peierls−Hubbard model is used to explain the electronic states, in which the transfer integral (t), the on-site and nearest neighbor-site Coulomb repulsions (U and V, respectively), and the electron−lattice interaction (S), all compete for energy.[17,18] The Pd and Pt complexes with a −X···M^{II} ···X−M^{IV}−X··· Peierls distorted 1D structure are generally present in a mixed-valence charge-density-wave (MV−CDW) state due to a large S value ($S > U$; Figure 1a). Moreover, Pd and Pt complexes in

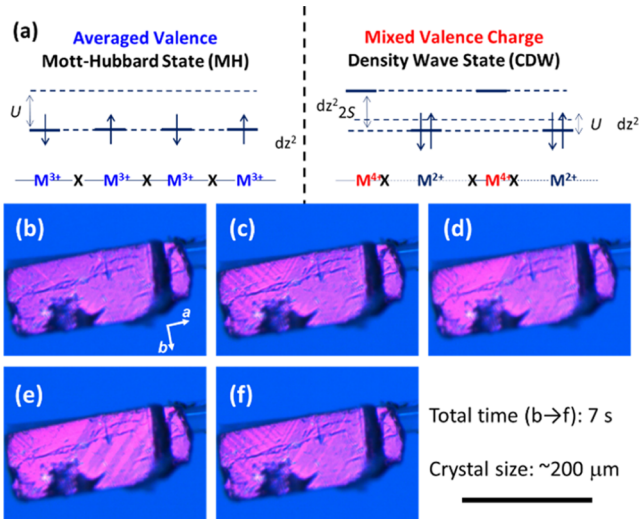

Figure 1. (a) Electronic state of quasi-one-dimensional halogen-bridged metal complexes. (b−f) Phase separation between MV−CDW and AV−MH at 141 K in a fluctuated N_2 gas flow (see Movie S1).

MV−CDW states have been extensively studied due to their chemical and physical properties, which include intervalence charge transfer from M^{II} to M^{IV} ions,[19] overtone progression of the resonance Raman mode,[20,21] soliton and polaron dynamics,[22,23] and two-leg ladder and square tubular skeletons formed by supramolecular assembly.[24,25] In contrast, it has been shown that Ni complexes have a −X−Ni^{III}−X−Ni^{III}−X− 1D structure and are in an averaged-valence Mott−Hubbard (AV−MH) state due to a large U value ($U > S$; Figure 1a).[26] Moreover, intriguing physical properties, such as enormous third-order nonlinear optical susceptibility,[27] negative differential electrical conductivity,[28] electrostatic carrier doping,[29] and spin-Peierls transitions,[30] have been reported.

Recently, several Pd complexes exhibiting MV−CDW to AV−MH CTPT (Peierls transition), in which the decrease in the Pd···Pd distances at low temperatures causes a decreases in the S value and the U value remains nearly constant in one complex, causing the Pd complex to transition to the AV−MH state, have been reported.[31,32] In particular, [Pd(cptn)$_2$Br]Br$_2$ (**1**) is the only system in the organic−inorganic hybrid molecular solid in which MV−CDW and AV−MH states coexist on the micrometer-order against the (±1 ± 1 0) plane over a broad temperature range (50−130 K).[33] In addition, without the use of a polarizer, a dynamic to-and-fro visible phase transition/separation can be observed in a fluctuating N_2 gas flow (Figure 1b−f, Movie S1: the brighter domain is in a MH state and the darker domain is in a CDW state). Furthermore, in scanning tunneling microscopy (STM) images, a phase separation is observed at the nanoscale.[34] In this temperature range, **1** exhibits a typical ferroelastic phase separation, comprising a CDW−MH quasi-epitaxial single crystal (close to homoepitaxial from the perspective of a single crystal[35,36]). Typical ferroelastics have a large band gap (~2.7 eV) in an inorganic system.[37] Xiong et al. have recently reported an organic−inorganic organometallic semiconductor with a narrow optical gap (ferrocenium tetrachloroferrate [Fe(Cp)$_2$][FeCl$_4$]) (1.61 eV).[38] However, **1** has a gap of less than half (0.60 and 0.43 eV) that value and thus has the potential to enable fast-response (to thermal, mechanical, and optical stimuli) and low-gap optical devices. Although the decrease in the energy gap also leads to difficulty in controlling the transition, **1** can be controlled by a hydrogen-bonding network.

To design molecular compounds with two or more phases in a single component, it is critical to understand the electron−lattice correlation and phase separation in a CTPT. However, discussing the mechanism at the atomic level is complicated because **1** in an MV−CDW state (at a higher temperature) has a superstructure with diffused scattering and phase separation,[39] making the extraction of structural information for each coexisting domain difficult. In this work, we determined the superstructure of an MV−CDW state using single-crystal X-ray diffraction and the coexisting structures using synchrotron powder X-ray diffraction. We showed that the Pd^{II}−Pd^{IV}/Pd^{III}−Pd^{III} phase transition and phase separation mechanism for [Pd(cptn)$_2$Br]Br$_2$ were propagated via a hydrogen-bonding network. In addition, the effects of the phase separation on the physical properties, such as spin susceptibility and conductivity, were clarified to better understand the behavior of the CDW−MH quasi-epitaxial crystal.

RESULTS AND DISCUSSION

Nanoscale Structure. To aid comprehension, we have included a breakdown of the structure here (CCDC no. 1449578).[33,39] Figure 2 and Table S1 show the crystal structure and crystal data for **1** at 93 K (**1** is in an AV−MH state). The complex crystallized in the $I222$ space group with the Pd ion in an elongated octahedral coordination sphere and the Br anion bridging square planar Pd(cptn)$_2$ moieties to form a linear chain along the a-axis (Figure 2a). The Pd−Pd distance within the chain was determined to be 5.22 Å. These chains formed a 2D sheet parallel to the ab plane via hydrogen bonding among free Br$^-$ counteranions and in-plane cptn ligands via a N−H···Br···H−N hydrogen-bonding network along the b axis (Figure 2b,c). These sheets were stacked along the c axis via van der Waals interactions and C−H···Br···H−C hydrogen bonding (Figure S1).

Diffuse scattering at $h = m + 0.5$ (m is an integer) [it contains additional structural information (superstructure)]

https://doi.org/10.1021/acs.inorgchem.2c02078
Inorg. Chem. 2022, 61, 14067−14074

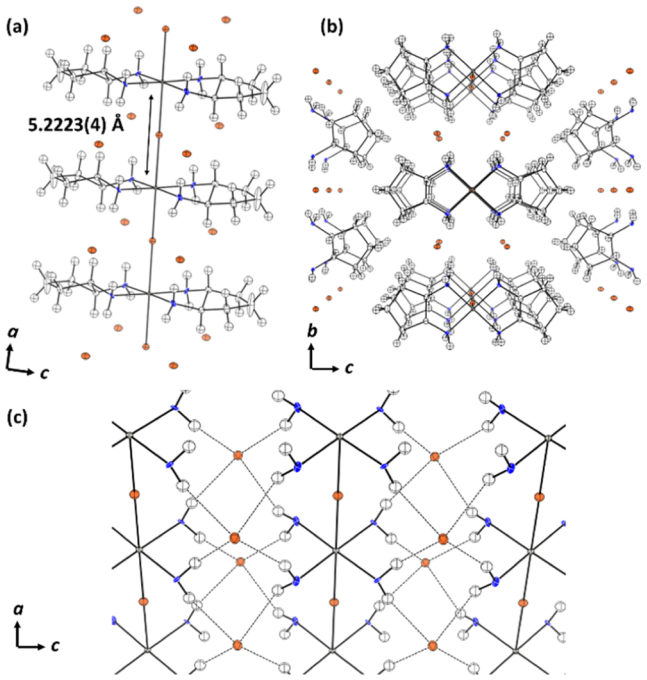

Figure 2. Crystal structure of **1** at 93 K. (a) 1D chain structure, (b) stacking structure, and (c) hydrogen-bonding network. Gray: Pd, Orange: Br, Blue: N, White: C, White(isotropy): H.

was observed in the MV−CDW state (higher temperature) (Figure S2). The three-dimensional-delta pair distribution function (3D-ΔPDF), a type of Patterson function, was used to analyze diffuse scattering.[39] In comparison to the structure in the AV−MH state, the structure in the MV−CDW state differs in three ways: (i) −Br···Pd^{II} ···Br−Pd^{IV}−Br··· Peierls distorted 1D structure; (ii) dimerization of Br^- counteranion; and (iii) local-ordering of C−H···Br···H−C hydrogen bonding.

(i) In the MV−CDW state, the structure contains −Br···Pd^{II} ···Br−Pd^{IV}−Br··· units with a Peierls distorted 1D structure. For the MV−CDW state, the electron−lattice interactions cause the displacement of the bridged Br anion from the center. At 260 K, from 3D-ΔPDF, the Pd^{II} ···Br and Br−Pd^{IV} distances were determined to be 2.76 and 2.49 Å, respectively (intrachain Pd−Pd distance was 5.25 Å).[39] Correlations between chains along the *b* axis correspond to the in-phase ordering of the −Br···Pd^{II} ···Br−Pd^{IV}−Br··· chains, whereas correlations along the *c* axis have almost no charge ordering (Figure S3). (ii) The Br^- counteranions dimerize along the *a* axis with pairs of counteranions moving in the Pd^{IV} direction by 0.035 Å (Figure S3).[39] This is because the in-plane cptn ligand has a long Pd^{IV}−N coordination distance and a short Pd^{II}−N coordination distance, allowing it to attract and repel Br^- counteranions via N−H···Br···H−N hydrogen bonding. The displacements of the Br^- counteranions serve as the starting point for phase transition propagation. (iii) Although the C5 atom was disordered in the AV−MH state, it was ordered and shifted in the Pd^{IV} direction in the MV−CDW state. This disorder occurs as a result of C5 atoms moving in the Pd^{IV} direction due to C−H···Br···H−C hydrogen bonding (These Br^- counteranions correlate with the adjacent MX chain, as shown in Figure S1). As discussed in the Supporting Information, there is no ferroelasticity along the *c* axis, which is connected to the domain of the *ab* plane. However, it does produce a weak correlation along the *c* axis.

Figure 3 depicts the sum of the diffuse scattering intensities at various temperatures. Cooling reduced the intensity,

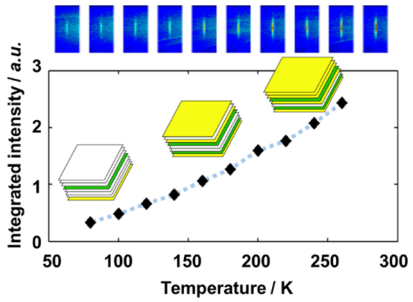

Figure 3. Sum of the diffuse scattering intensities at various temperatures. Each plate represents a 2D sheet along the *ab* plane. The green and yellow plates represent the CDW domains; since there is almost no correlation among the 2D sheets along the *c* direction, they are represented by different colors in the diagram. The white plates represent the MH domains.

whereas the width of the diffuse scattering did not change. This behavior indicates that although the MV−CDW domain shrinks, the structure and correlation length in the domain are the same.

We measured the synchrotron powder X-ray diffraction pattern (PXRD) of **1** in a temperature range to confirm the boundary between AV−MH and MV−CDW (Figure S4). For the temperatures depicted in Figure 4, the diffraction peak

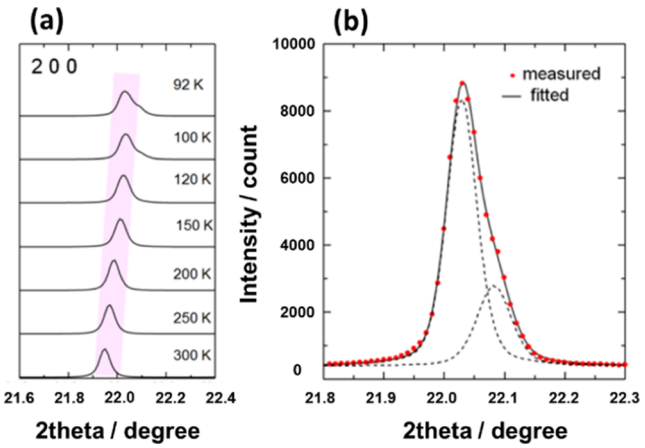

Figure 4. PXRD pattern of the peak of the (2 0 0) plane of **1** (a) at various temperatures and (b) at 92 K during the cooling process.

corresponds to the (2 0 0) plane. A single peak (without any shoulder peak) was observed between 120 and 300 K, and an additional shoulder peak appeared between 92 and 100 K. These single and shoulder peaks correspond to the Pd···Pd distances of the MV−CDW and AV−MH, respectively. The single and shoulder peaks at (2 0 0) were deconvoluted into two peaks in the ratio of 3:1 (CDW/MH) (this ratio was calculated using bulk sample, and this tendency might not always match the behavior of a single crystal because it was obtained as an average of several crystals) At 92 K, the unit cells were fit to be CDW (*a*: 5.231, *b*: 6.960, and *c*: 22.623 Å) and MH (*a*: 5.219, *b*: 6.967, and *c*: 22.607 Å) using the Le Bail method (R = 4.47%, Figure S5; see the methods section). The difference in the Pd···Pd distances in the MH and CDW states ($|\Delta a|$) was only 0.012 Å. This value is less than that reported

https://doi.org/10.1021/acs.inorgchem.2c02078
Inorg. Chem. 2022, 61, 14067−14074

for the Pd complex with alkyl chain (~0.03 Å).[31] In addition, the distance between the chains along the *b* axis increased from the MV−CDW to AV−MH states. These findings confirmed that there is only a slight difference in the value of unit cell parameters between the MV−CDW and AV−MH states.

STM images are shown in Figure 5. We observed atomic-scale phase separation between the MV−CDW and AV−MH

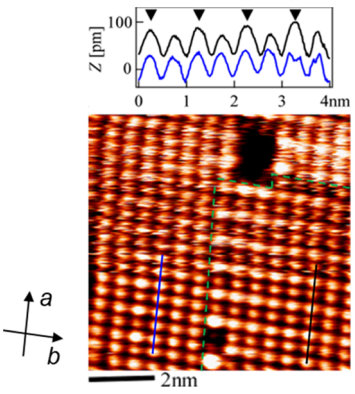

Figure 5. STM image of **1** at 113 K. The blue, black, and green dotted lines indicate the AV−MH state, the MV−CDW state, and the boundary between them, respectively.

domains over an area of 25 nm × 25 nm. Bright spots were observed on the Pd^{IV} site in the MV−CDW domain and on the Pd^{III} site in the AV−MH domain (Figure S6).[34] Although the difference in the CDW $Pd^{(IV-\rho)}$−Br···$Pd^{(II+\rho)}$ and MH Pd^{III}−X−Pd^{III} electronic states is small (ρ is almost 1), two domains with clear borders were observed at 113 K. On the other hand, the Ni−Pd heterojunction system has three domains, where the intermediate domain cannot be distinguished whether MV−CDW or AV−MH.[40] These heterojunction interface differences may require attention in fabricating devices. The borderline is not parallel to the (1 1 0) plane that is observed in the macroscale structure, as shown in Figure S7, but it is parallel to the (1 0 0) or (0 1 0) plane at the nanoscale and is adjacent to the defects. These findings indicated that the defects act as nanoscale anchors for the domain wall. At the same time, we observed quasi-epitaxial growth at the nanoscale between the MV−CDW and AV−MH states.

Macroscale Structure. Figure S7 shows optical images of a single crystal of **1** on the substrate at various temperatures. At temperatures between 50 and 130 K, there is a phase separation between the bright and dark domains, whose border is parallel to the (110) plane. In addition, the bright and dark domains were assigned to MV−CDW and AV−MH states, respectively, using Raman spectroscopy.[33] In Figure S8, the ratio of the AV−MH domain is plotted (the optical images in Figure S7 were used to calculate this ratio, where the bright and dark domains correspond to the CDW and MH states, respectively). A thin crystal in a N_2 gas flow at 141 K (±2 K) underwent dynamic phase transitions between MV−CDW and AV−MH states with a striped domain (Movie S1; the colors in Figure S7 and the movie are different due to the use of different cameras and light sources). On the other hand, at a given temperature, the phase separation in the crystals on the substrate was static because the thermal conductivity of **1** is sufficient to follow the surrounding environment. In addition, the pattern was basically independent of the direction of the flow (Movies S2 and S3 at 135 K). The front and back sides of the crystals have similar striped domains (Movies S2 and S3 at 135 K). These findings indicate that the domain of the striped pattern is correlated with the depth direction (see Supporting Information before Figure S9 and Table S2). Moreover, the domain shape of each crystal is memorized, and as will be described later, can be changed by an external force.

Propagation Mechanism for the Phase Transition. From PXRD and optical conductivity measurements, there was a decrease in the Pd−Pd distance of 0.013 Å induced by the transition from the CDW to MH state and a 0.2 eV optical gap fluctuation. To comprehend the ferroelastic phenomena, we must consider two dimensions: (i) microscopic and (ii) macroscopic. In other words, there are specific trends along the *a* and *b* axes when the averaged structures around the counteranions are compared at room temperature (~300 K) (MV−CDW) and 93 K (AV−MH) (Figure 6).

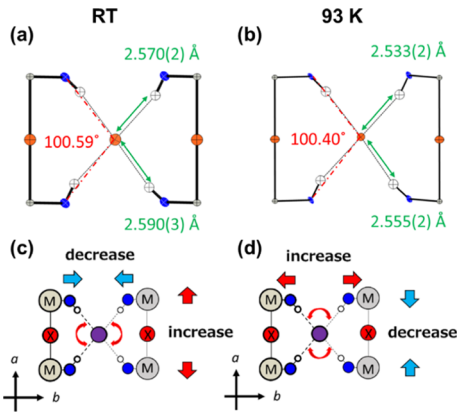

Figure 6. Hydrogen bonding structure of **1** (a), (c) at RT, and (b), (d) at 93 K. (a) and (b) Gray: Pd, Orange: Br, Blue: N, White: H. (c) and (d) Gray: Pd, Red: bridged Br, Purple: Br counteranion, Blue: N, White: H.

(i) At room temperature, the N(A)···Br···N(B) angle was 100.59°, whereas it was 100.40° at 93 K. A comparison of the MV−CDW and MH states indicated that both the Pd···Pd distance (*a* direction) and the N(A)···Br···N(B) angle increased and the interchain (*b* axis) distance decreased. In the AV−MH state, the converse occurred, as confirmed by the temperature dependence of the unit cell (Figure S10). Thus, in the MV−CDW state, there is spontaneous strain along the *a* direction, whereas in the AV−MH state, there is spontaneous strain along the *b* direction. These strains act as stresses on the overall thermal strain of the crystal. Therefore, the NH···Br···HN hydrogen bond adjusts and propagates the strain along the *a* and *b* directions during the transition, similar to a jack. In the MV−CDW state, Br counteranions are shifted by 0.035 Å along the *a* direction. Therefore, the structural change is highly complicated. The polarities of $N^{\delta-}$−$H^{\delta+}$ bond generally follow the order $(Pd^{II}\cdots)N^{\delta-}$−$H^{\delta+}$ < $(Pd^{III}\cdots)N^{\delta\prime-}$−$H^{\delta\prime+}$ < $(Pd^{IV}\cdots)$-$N^{\delta\prime\prime-}$−$H^{\delta\prime\prime+}$. Dimerization of the Br^- counteranion may be induced by the difference in the $N^{\delta-}$−$H^{\delta+}$···Br^-···$H^{\delta+}$−$N^{\delta-}$ hydrogen bonding, as determined from the 3D-ΔPDF results. When a chain transitions to the AV−MH state, the $Pd^{(II\rightarrow III)}$NH···Br hydrogen bond strengthens and its bond length decreases, whereas the $Pd^{(IV\rightarrow III)}$NH···Br hydrogen bond weakens and its bond length increases. Subsequently, the Br^- anion migrates toward the center. At this point, the

https://doi.org/10.1021/acs.inorgchem.2c02078
Inorg. Chem. 2022, 61, 14067−14074

(Pd^{IV}···)NH···Br and (Pd^{II}···)NH···Br hydrogen bond lengths increase and decrease in the neighboring chains, respectively. These structural modifications to the ligands perturbate the dz^2 orbitals of the Pd ion (the dz^2 = $d(2z^2-x^2-y^2)$ orbital also contributes to the xy plane). Furthermore, this perturbation induces a phase transition in the subsequent chains. As a result, hydrogen bonding is critical for phase separation and transition.

(ii) The differences in a ($|\Delta a|$) and b ($|\Delta b|$) axes of the MV−CDW and AV−MH states were calculated to be 0.012 and 0.007 Å, respectively, using PXRD data at 92 K. The sums of these differences were 0.24 and 0.14 μm in a complete crystal (~100 μm which corresponds to approximately 2.0 × 10^4 units for each axis) (eq S1). Contrastingly, the difference in $|\Delta c|$ between CDW and MH at 92 K was calculated to be 0.016 Å. In the case of the c axis, the sum of difference was 7.2 nm for a complete crystal (~10 μm which corresponds to approximately 4.5 × 10^3 units for each axis) (eq S1). These differences immediately relax if each domain is in paraelastics. Each domain, however, alleviates the strain by moving the domain wall. This behavior is typical of the ferroelastic domain. The total spontaneous strain was calculated as $s_{total} = (s_{a(CDW \rightarrow MH)}{}^2 + s_{b(CDW \rightarrow MH)}{}^2 + s_{c(CDW \rightarrow MH)}{}^2)^{1/2} = 0.0026$, where $|s_{a(CDW \rightarrow MH)}| = |(a_{MH} - a_{CDW})/a_{CDW}| = 0.0023$, $|s_{b(CDW \rightarrow MH)}| = |(b_{MH} - b_{CDW})/b_{CDW}| = 0.0010$, and $|s_{c(CDW \rightarrow MH)}| = |(c_{MH} - c_{CDW})/c_{CDW}| = 0.0007$. These values are comparable to those reported for typical ferroelastics.[41,42] The domain wall corresponding to the (1 1 0) plane of each domain [$d_{CDW} = (a_{CDW}{}^2 + b_{CDW}{}^2)^{1/2} = 8.707$ Å, $d_{MH} = (a_{MH}{}^2 + b_{MH}{}^2)^{1/2} = 8.705$ Å] has almost no epitaxial strain.[42]

The interactions between cptn ligands are weak along the c axis, where the flexible alkylene ring may release the epitaxial strain. In addition, by applying external strain, the domain wall can be eliminated (Figure 7, Movie S4. The crystal was manually pushed using the needle at 100 K). Initially, the role of hydrogen bonding in the bulk appears ambiguous. Nonetheless, when considering nanoscale functionality, the sum of the innumerable hydrogen bonds promotes phase separation in the bulk.

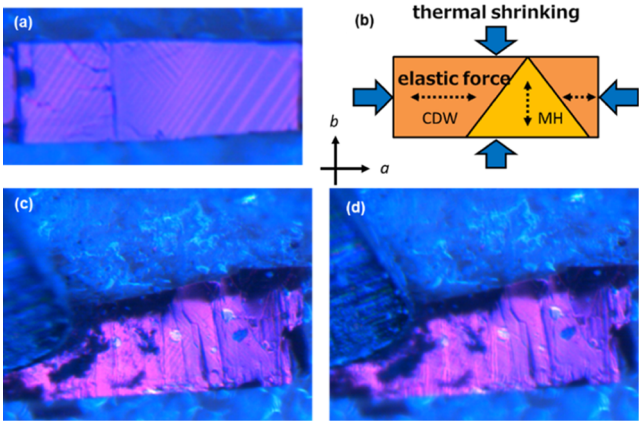

Figure 7. Images of a single crystal of **1**. (a) At 110 K, (c) at 100 K before push, and (d) at 100 K after push. (b) Schematic illustration of the thermal shrinking of the single crystal and its elastic force (spontaneous strain).

Physical Properties. The charge transfer energy (E_{CT}; optical gap is calculated from the reflectivity spectra of **1** at various temperatures, shown in Figure S11) versus T plots of **1** at various temperatures are shown in Figure 8. The E_{CT} in the MV−CDW state corresponds to CT from an occupied band of the Pd^{II} dz^2 orbital to an unoccupied band of the Pd^{IV} dz^2 orbital and is defined as $2S-U$, where S is proportional to the Pd···Pd distance. Moreover, E_{CT} in the MH state corresponds to CT from the occupied lower Hubbard band of the Pd^{III} dz^2 orbital to the unoccupied upper Hubbard band of the Pd^{III} dz^2 orbital and is defined as U, where U is on-site Coulomb repulsion energy.[23] The E_{CT} decreased gradually from 0.66 to 0.60 eV between 300 and 150 K and abruptly decreased from 0.60 to 0.43 eV between 150 and 100 K. Then, E_{CT} was nearly constant at 0.43 eV between 100 and 10 K; this value is consistent with the previously reported value (~0.45 eV).[43] This small E_{CT} value or U value is attributed to the dz^2 orbital expansion induced by the weak ligand field of the in-plane ligands. These results indicate that a CDW-to-MH transition occurs between 150 and 100 K, and that the difference in E_{CT} values for CDW and MH is at least 0.17 eV.

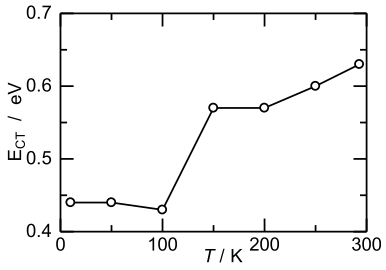

Figure 8. E_{CT} vs T plots of **1** at various temperatures.

Figure S12a shows the temperature dependence of the spin susceptibility in **1**, as determined by electron spin resonance. We observed a clear change in the spin susceptibility at approximately 150 K. In the low-temperature phase, a Curie-like behavior was observed, as shown by the dashed curve. These Curie spins could arise from the chain ends or the segments containing odd number of spins in the Pd^{III} MH state (S = 1/2) because of antiferromagnetic interaction. Contrastingly, spin susceptibility decreased remarkably at the high-temperature phase, demonstrating the dominance of the nonmagnetic Pd^{II}−Pd^{IV} CDW state. Considering the entropy of the spin (CDW state < MH state), the spin should have high entropy in the high-temperature phase. In contrast, the MX complexes have high spin entropy (MH state) in the low-temperature phase because the structural change (decrease in the Pd···Pd distances) occurring in this phase is dominant in the CDW-to-MH transition of Pd-based MX complexes.[44] At the intermediate temperature region of 200−100 K, the spin susceptibility changed significantly with blunt hysteresis due to the formation of the phase separation. $1/\chi$ versus T plots for **1** are shown in Figure S12b. The spin concentration below 100 K is calculated as 0.36%, which is higher than that of reported Pd-based MX complexes (~0.14%).[31,43]

In Figure 9, the electrical conductivities (σ) of **1** and $[Pd(chxn)_2Br]Br_2$ at various temperatures (T) are plotted. At 300 K, the conductivity of **1** was 10^{-2} S cm^{-1}, which is the second highest value of all Pd-based MX compounds[43] reported so far and significantly higher than that of ferrocenium tetrachloroferrate [~10^{-6} S cm^{-1} (AC)].[38] This higher conductivity is facilitated by the lower band gap and 2D sheet structure, wherein the defects can be bypassed when electron conduction occurs through a one-dimensional chain.

https://doi.org/10.1021/acs.inorgchem.2c02078
Inorg. Chem. 2022, 61, 14067−14074

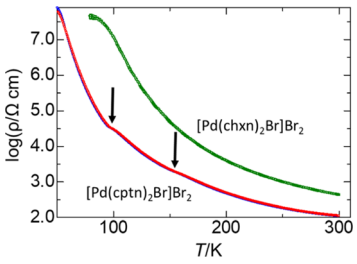

Figure 9. Electrical conductivities (σ) of **1** and $[Pd(chxn)_2Br]Br_2$ at various temperatures.

The conductivity of **1** then decreased upon cooling, which is typical for semiconductors. In $\ln(\sigma)$ versus $T^{-1} \times 10^3$ plots (Arrhenius plots), the activation barrier (E_a) is nearly constant at 145 meV compared to 227 meV for $[Pd(chxn)_2Br]Br_2$ at low temperatures. There are shoulder peaks near 6.5 and 10 $K^{-1} \times 10^3$ (~150 and ~100 K), which appear to reduce E_a. Although this behavior could be explained by the fact that the crystals are quasi-heterojunctions, it is still being investigated. Because the optical gaps for the MV−CDW and AV−MH states are 0.4 and 0.6 eV, respectively, and the difference between them is small (~0.2 eV), the interface may be highly conductive.

Ferroelastic phase separation induces the behavior of the physical properties.[45−49] Hence, it would be advantageous if the physical properties of the compound could be spontaneously controlled via molecular design.

CONCLUSIONS

In this study, for the first time, we elucidated the mechanism of $Pd^{II}-Pd^{IV}/Pd^{III}-Pd^{III}$ phase transition and the phase separation mechanism of **1** at the atomic and molecular levels using synchrotron X-ray techniques. The N−H···Br···H−N hydrogen bonds propagated the strain that induced the transition like a jack. The dynamic to-and-fro visible phase transition/separation was derived from spontaneous strain and temperature fluctuations. The differences in the Pd···Pd distance and optical gap of the AV−MH and MV−CDW were only 0.012 Å and 0.17 eV, respectively. These differences could be elucidated only via methods such as X-ray diffraction using a synchrotron radiation source. In addition, the effects of the phase separation on the physical properties, such as spin susceptibility and electrical conductivity, were clarified to understand the behavior of CDW−MH quasi-epitaxial crystal. Finally, the phase separation was caused by ferroelasticity through the hydrogen-bonding network, and it could be controlled by applying an external force. These findings imply that spin magnetic susceptibility and electrical conductivity can be manipulated as well. We expect that these results will enable the design of more rational molecular devices.

EXPERIMENTAL SECTION

$[Pd(cptn)_2Br]$ Br_2 (**1**) was synthesized using the same procedure as described previously.[33] X-ray diffraction patterns of single crystals were collected using a Bruker APEX-II diffractometer equipped with an APEX II CCD detector and a JAPAN Thermal Engineering Co., Ltd. Cryo system DX-CS190LD. The synchrotron single-crystal X-ray diffraction data were collected on the NW2A Beamline in the Photon Factory Advanced Ring of the High Energy Accelerator Research Organization (KEK, Proposal no. 2014G008), the Swiss-Norwegian Beamlines (SNBL) in European Synchrotron Radiation Facility (ESRF), and the 2D Beamline in Pohang Accelerator Laboratory (PAL) (λ = 0.700 Å). The synchrotron powder-crystal X-ray diffraction data were collected on the BL02B2 Beamline in SPring-8 (λ = 1.000 Å). The Le Bail analysis[48] was performed using the Rietica program package (old version). Temperature dependence of STM was analyzed using an Omicron LT-STM with an electrochemically etched W tip. The Fourier transform infrared spectra of single crystal were measured in reflectance mode using a JASCO FT/IR 6700 spectrometer in conjunction with an IRT-5000 microscope unit. Polarized reflectivity spectra in the UV−Vis−NIR range were acquired using a custom-built spectrometer equipped with a 25 cm grating monochromator and an optical microscope. Temperature regulation was accomplished using a Janis ST-300 cryostat equipped with a ZnSe window. The Kramers−Kronig transformation was used to convert the obtained reflectivity spectra to optical conductivity spectra. A Quantum Design PPMS MODEL 6000 was used to determine the electrical conductivity.

ASSOCIATED CONTENT

Supporting Information

The Supporting Information is available free of charge at https://pubs.acs.org/doi/10.1021/acs.inorgchem.2c02078.

Crystal data, structural information, PXRD data, STM images, images of crystal, optical data, and magnetic properties (PDF)

Phase separation between MV−CDW and AV−MH at 141 K in a fluctuated N_2 gas flow (MP4)

Imaging of a single crystal at 135 K (MP4)

Imaging of a single crystal at 135 K (MP4)

Imaging of a single crystal at 110 K (MP4)

AUTHOR INFORMATION

Corresponding Authors

Takefumi Yoshida − *Department of Chemistry, Graduate School of Science, Tohoku University, Sendai, Miyagi 980-8578, Japan;* Present Address: Innovation Research Center for Fuel Cells, The University of Electro-Communications, Chofu, Tokyo 182-8585, Japan; orcid.org/0000-0003-3479-7890; Email: takefumi.yoshida.b7@tohoku.ac.jp

Shinya Takaishi − *Department of Chemistry, Graduate School of Science, Tohoku University, Sendai, Miyagi 980-8578, Japan;* orcid.org/0000-0002-6739-8119; Email: shinya.takaishi.d8@tohoku.ac.jp

Masahiro Yamashita − *Department of Chemistry, Graduate School of Science, Tohoku University, Sendai, Miyagi 980-8578, Japan; School of Materials Science and Engineering, Nankai University, Tianjin 300350, China;* Email: yamasita.m@gmail.com

Authors

Laurent Guérin − *Institut de Physique de Rennes, Rennes Cedex 35042, France*

Tatsuhiro Kojima − *Department of Chemistry, Graduate School of Science, Osaka University, Toyonaka, Osaka 560-0043, Japan;* orcid.org/0000-0002-1313-8987

Hiroyoshi Ohtsu − *Department of Chemistry, School of Science, Tokyo Institute of Technology, Tokyo 152-8550, Japan;* orcid.org/0000-0002-2911-3151

Masaki Kawano − *Department of Chemistry, School of Science, Tokyo Institute of Technology, Tokyo 152-8550, Japan;* orcid.org/0000-0001-9886-4226

Tatsuya Miyamoto − *Department of Advanced Materials Science, Graduate School of Frontier Sciences, The University of Tokyo, Kashiwa 277-8561, Japan*

Hiroshi Okamoto − *Department of Advanced Materials Science, Graduate School of Frontier Sciences, The University of Tokyo, Kashiwa 277-8561, Japan;* orcid.org/0000-0003-2807-5277
Kenichi Kato − *RIKEN SPring-8 Center, Sayo-gun, Hyogo 679-5148, Japan*
Masaki Takata − *Institute of Multidisciplinary Research for Advanced Materials, Tohoku University, Sendai 980-8577, Japan*
Yuka Hosomi − *Faculty of Pure and Applied Sciences, University of Tsukuba, Tsukuba 305-8573, Japan*
Shoji Yoshida − *Faculty of Pure and Applied Sciences, University of Tsukuba, Tsukuba 305-8573, Japan*
Hidemi Shigekawa − *Faculty of Pure and Applied Sciences, University of Tsukuba, Tsukuba 305-8573, Japan;* orcid.org/0000-0001-9550-5148
Hisaaki Tanaka − *Department of Applied Physics, Graduate School of Engineering, Nagoya, University, Nagoya 464-8603, Japan;* orcid.org/0000-0003-3503-6161
Shin-ichi Kuroda − *Department of Applied Physics, Graduate School of Engineering, Nagoya, University, Nagoya 464-8603, Japan*
Hiroaki Iguchi − *Department of Chemistry, Graduate School of Science, Tohoku University, Sendai, Miyagi 980-8578, Japan;* orcid.org/0000-0001-5368-3157
Brian K. Breedlove − *Department of Chemistry, Graduate School of Science, Tohoku University, Sendai, Miyagi 980-8578, Japan;* orcid.org/0000-0003-1419-577X
Zhao-Yang Li − *School of Materials Science and Engineering, Nankai University, Tianjin 300350, China;* orcid.org/0000-0002-0952-9862

Complete contact information is available at: https://pubs.acs.org/10.1021/acs.inorgchem.2c02078

Author Contributions

The manuscript was written through contributions of all authors.

Notes

The authors declare no competing financial interest.

■ ACKNOWLEDGMENTS

This work was partially supported by JSPS KAKENHI grants JP19H05631, JP20K15293, and JP21H04988 and the National Natural Science Foundation of China (NSFC, 22150710513). The synchrotron single-crystal X-ray diffraction data were collected on the NW2A Beamline in the Photon Factory Advanced Ring of the High Energy Accelerator Research Organization (KEK, Proposal no. 2014G008), the SNBL in ESRF, and on the 2D Beamline in PAL. The synchrotron powder-crystal X-ray diffraction data were collected on the BL02B2 Beamline in SPring-8. P. M.Y. acknowledges the support of the 111 project (B18030) from China.

■ REFERENCES

(1) Cowburn, R. P.; Welland, M. E. Room Temperature Magnetic Quantum Cellular Automata. *Science* **2000**, *287*, 1466−1468.
(2) Koyama, T.; Chiba, D.; Ueda, K.; Kondou, K.; Tanigawa, H.; Fukami, S.; Suzuki, T.; Ohshima, N.; Ishiwata, N.; Nakatani, Y.; Kobayashi, K.; Ono, T. Observation of the intrinsic pinning of a magnetic domain wall in a ferromagnetic nanowire. *Nat. Mater.* **2011**, *10*, 194−197.
(3) Fiebig, M.; Lottermoser, T.; Fröhlich, D.; Goltsev, A. V.; Pisarev, R. V. Observation of coupled magnetic and electric domains. *Nature* **2002**, *419*, 818−820.
(4) Kagawa, F.; Horiuchi, S.; Minami, N.; Ishibashi, S.; Kobayashi, K.; Kumai, R.; Murakami, Y.; Tokura, Y. Polarization Switching Ability Dependent on Multidomain Topology in a Uniaxial Organic Ferroelectric. *Nano Lett.* **2014**, *14*, 239−243.
(5) Wei, X.-K.; Sluka, T.; Fraygola, B.; Feigl, L.; Du, H.; Jin, L.; Jia, C.-L.; Setter, N. Controlled Charging of Ferroelastic Domain Walls in Oxide Ferroelectrics. *ACS Appl. Mater. Interfaces* **2017**, *9*, 6539−6546.
(6) Fan, Z.; Xue, F.; Tutuncu, G.; Chen, L.-Q.; Tan, X. Interaction Dynamics Between Ferroelectric and Antiferroelectric Domains in a $PbZrO_3$-Based Ceramic. *Phys. Rev. Appl.* **2019**, *11*, 064050.
(7) Hu, Y.; You, L.; Xu, B.; Li, T.; Morris, S. A.; Li, Y.; Zhang, Y.; Wang, X.; Lee, P. S.; Fan, H. J.; Wang, J. Ferroelastic-switching-driven large shear strain and piezoelectricity in a hybrid ferroelectric. *Nat. Mater.* **2021**, *20*, 612−617.
(8) Sasaki, T.; Sakamoto, S.; Takasaki, Y.; Takamizawa, S. A Multidirectional Superelastic Organic Crystal by Versatile Ferroelastical Manipulation. *Angew. Chem., Int. Ed.* **2020**, *132*, 4370−4373.
(9) Takamizawa, S.; Takasaki, Y. Versatile Shape Recoverability of Odd-Numbered Saturated Long-Chain Fatty Acid Crystals. *Cryst. Growth Des.* **2019**, *19*, 1912−1920.
(10) Kumai, R.; Okimoto, Y.; Tokura, Y. Current-Induced Insulator-Metal Transition and Pattern Formation in an Organic Charge-Transfer Complex. *Science* **1999**, *284*, 1645−1647.
(11) Okimoto, Y.; Kumai, R.; Saitoh, E.; Izumi, M.; Horiuchi, S.; Tokura, Y. Spectroscopic study of stripe pattern formation induced by current injection in a charge-transfer complex. *Phys. Rev. B: Condens. Matter Mater. Phys.* **2004**, *70*, 115104.
(12) Sasaki, T.; Yoneyama, N.; Suzuki, A.; Kobayashi, N.; Ikemoto, Y.; Kimura, H. Real Space Imaging of the Metal−Insulator Phase Separation in the Band Width Controlled Organic Mott System κ-(BEDT-TTF)2Cu[N(CN)2]Br. *J. Phys. Soc. Jpn.* **2005**, *74*, 2351−2360.
(13) Pustogow, A.; McLeod, A. S.; Saito, Y.; Basov, D. N.; Dressel, M. Internal strain tunes electronic correlations on the nanoscale. *Sci. Adv.* **2018**, *4*, No. eaau9123.
(14) Yoshida, T.; Takaishi, S.; Kumagai, S.; Iguchi, H.; Mian, M. R.; Yamashita, M. Observation of charge bistability in quasi-one-dimensional halogen-bridged palladium complexes by X-ray absorption spectroscopy. *Dalton Trans.* **2019**, *48*, 11628−11631.
(15) Matsuzaki, H.; Iwata, M.; Miyamoto, T.; Terashige, T.; Iwano, K.; Takaishi, S.; Takamura, M.; Kumagai, S.; Yamashita, M.; Takahashi, R.; Wakabayashi, Y.; Okamoto, H. Excitation-Photon-Energy Selectivity of Photoconversions in Halogen-Bridged Pd-Chain Compounds: Mott Insulator to Metal or Charge-Density-Wave State. *Phys. Rev. Lett.* **2014**, *113*, 096403.
(16) Yamashita, M.; Okamoto, H., *Material Designs and New Physical Properties in MX- and MMX-Chain Compounds*; Springer: Berlin, 2012.
(17) Nasu, K. Extended Peierls-Hubbard Model for One-Dimensional N-Sites N-Electrons System. I. Phase Diagram by Mean Field Theory. *J. Phys. Soc. Jpn.* **1983**, *52*, 3865−3873.
(18) Weber-Milbrodt, S. M.; Gammel, J. T.; Bishop, A. R.; Loh, E. Y. Two-band model for halogen-bridged mixed-valence transition-metal complexes. II. Electron-electron correlations and quantum phonons. *Phys. Rev. B: Condens. Matter Mater. Phys.* **1992**, *45*, 6435−6458.
(19) Clark, R. J. H.; Kurmoo, M. Electronic and resonance Raman spectra of mixed-valence linear-chain complexes of platinum with 1,3-diaminopropane. *Inorg. Chem.* **1980**, *19*, 3522−3527.
(20) Clark, R. J. H.; Frank, M. L.; Trunble, W. R. Resonance Raman spectra and excitation profiles of the mixed valence compound wolffram's red $[Pt^{II}(C_2H_5NH_2)_4][Pt^{IV}(C_2H_5NH_2)_4Cl_2]Cl_4 4H_2O$. *Chem. Phys. Lett.* **1976**, *41*, 287−292.
(21) Clark, R. J. H. Nyholm Lecture. Synthesis, structure, and spectroscopy of metal−metal dimers, linear chains, and dimer chains. *Chem. Soc. Rev.* **1990**, *19*, 107−131.

(22) Okamoto, H.; Yamashita, M. Solitons, Polarons, and Excitons in Quasi-One-Dimensional Halogen-Bridged Transition Metal Compounds. *Bull. Chem. Soc. Jpn.* **1998**, *71*, 2023−2039.
(23) Takaishi, S.; Kawakami, D.; Yamashita, M.; Sasaki, M.; Kajiwara, T.; Miyasaka, H.; Sugiura, K.-i.; Wakabayashi, Y.; Sawa, H.; Matsuzaki, H.; Kishida, H.; Okamoto, H.; Watanabe, H.; Tanaka, H.; Marumoto, K.; Ito, H.; Kuroda, S.-i. Dynamical Valence Fluctuation at the Charge−Density−Wave Phase Boundary in Iodide-Bridged Pt Compound [Pt(chxn)2I]I2. *J. Am. Chem. Soc.* **2006**, *128*, 6420−6425.
(24) Kawakami, D.; Yamashita, M.; Matsunaga, S.; Takaishi, S.; Kajiwara, T.; Miyasaka, H.; Sugiura, K.-i.; Matsuzaki, H.; Okamoto, H.; Wakabayashi, Y.; Sawa, H. Halogen-Bridged PtII/PtIV Mixed-Valence Ladder Compounds. *Angew. Chem., Int. Ed.* **2006**, *45*, 7214−7217.
(25) Kobayashi, A.; Kitagawa, H. Mixed-Valence Two-Legged MX-Ladder Complex with a Pair of Out-of-Phase Charge-Density Waves. *J. Am. Chem. Soc.* **2006**, *128*, 12066−12067.
(26) Toriumi, K.; Wada, Y.; Mitani, T.; Bandow, S.; Yamashita, M.; Fujii, Y. Synthesis and crystal structure of a novel one-dimensional halogen-bridged nickel(III)-X-nickel(III) compound, {[Ni(R,R-chxn)$_2$Br]Br$_2$}. *J. Am. Chem. Soc.* **1989**, *111*, 2341−2342.
(27) Kishida, H.; Matsuzaki, H.; Okamoto, H.; Manabe, T.; Yamashita, M.; Taguchi, Y.; Tokura, Y. Gigantic optical nonlinearity in one-dimensional Mott-Hubbard insulators. *Nature* **2000**, *405*, 929−932.
(28) Kishida, H.; Ito, T.; Nakamura, A.; Takaishi, S.; Yamashita, M. Current oscillation originating from negative differential resistance in one-dimensional halogen-bridged nickel compounds. *J. Appl. Phys.* **2009**, *106*, 016106.
(29) Takaishi, S.; Yamashita, M.; Matsuzaki, H.; Okamoto, H.; Tanaka, H.; Kuroda, S.-i.; Goto, A.; Shimizu, T.; Takenobu, T.; Iwasa, Y. One-Dimensional Bromo-Bridged NiIII Complexes [Ni(S,S-bn)2Br]Br2 (S,S-bn=2S,3S-diaminobutane): Synthesis, Physical Properties, and Electrostatic Carrier Doping. *Chem. - Eur. J.* **2008**, *14*, 472−477.
(30) Takaishi, S.; Tobu, Y.; Kitagawa, H.; Goto, A.; Shimizu, T.; Okubo, T.; Mitani, T.; Ikeda, R. The NQR Observation of Spin-Peierls Transition in an Antiferromagnetic MX-Chain Complex [NiBr(chxn)$_2$]Br$_2$. *J. Am. Chem. Soc.* **2004**, *126*, 1614−1615.
(31) Takaishi, S.; Takamura, M.; Kajiwara, T.; Miyasaka, H.; Yamashita, M.; Iwata, M.; Matsuzaki, H.; Okamoto, H.; Tanaka, H.; Kuroda, S.-i.; Nishikawa, H.; Oshio, H.; Kato, K.; Takata, M. Charge-Density-Wave to Mott−Hubbard Phase Transition in Quasi-One-Dimensional Bromo-Bridged Pd Compounds. *J. Am. Chem. Soc.* **2008**, *130*, 12080−12084.
(32) Yamashita, M. Next Generation Multifunctional Nano-Science on Advanced Metal Complexes with Quantum Effect and Non-linearity. *Bull. Chem. Soc. Jpn.* **2021**, *94*, 209−264.
(33) Yoshida, T.; Takaishi, S.; Iguchi, H.; Okamoto, H.; Tanaka, H.; Kuroda, S.-i.; Hosomi, Y.; Yoshida, S.; Shigekawa, H.; Kojima, T.; Ohtsu, H.; Kawano, M.; Breedlove, B. K.; Guérin, L.; Yamashita, M. Optically Visible Phase Separation between Mott-Hubbard and Charge-Density-Wave Domains in a Pd-Br Chain Complex. *ChemistrySelect* **2016**, *1*, 259−263.
(34) Yuka, H.; Shoji, Y.; Atsushi, T.; Takefumi, Y.; Shinya, T.; Osamu, T.; Masahiro, Y.; Hidemi, S. Temperature dependence of Peierls−Hubbard phase transition in [Pd(cptn) $_2$ Br]Br $_2$ studied by scanning tunneling microscopy. *Jpn. J. Appl. Phys.* **2016**, *55*, 08NB16.
(35) Wang, L.; King, I.; Chen, P.; Bates, M.; Lunt, R. R. Epitaxial and quasiepitaxial growth of halide perovskites: New routes to high end optoelectronics. *APL Mater.* **2020**, *8*, 100904.
(36) Zhang, H.; Qin, M.; Chen, Z.; Yu, W.; Ren, Z.; Liu, K.; Huang, J.; Zhang, Y.; Liang, Q.; Chandran, H. T.; Fong, P. W. K.; Zheng, Z.; Lu, X.; Li, G. Bottom-Up Quasi-Epitaxial Growth of Hybrid Perovskite from Solution Process—Achieving High-Efficiency Solar Cells via Template-Guided Crystallization. *Adv. Mater.* **2021**, *33*, 2100009.
(37) Farokhipoor, S.; Noheda, B. Conduction through 71̊ Domain Walls in $BiFeO_3$ Thin Films. *Phys. Rev. Lett.* **2011**, *107*, 127601.
(38) Zhang, H.-Y.; Hu, C.-L.; Hu, Z.-B.; Mao, J.-G.; Song, Y.; Xiong, R.-G. Narrow Band Gap Observed in a Molecular Ferroelastic: Ferrocenium Tetrachloroferrate. *J. Am. Chem. Soc.* **2020**, *142*, 3240−3245.
(39) Guérin, L.; Yoshida, T.; Zatterin, E.; Simonov, A.; Chernyshov, D.; Iguchi, H.; Toudic, B.; Takaishi, S.; Yamashita, M. Elucidating 2D Charge-Density-Wave Atomic Structure in an MX−Chain by the 3D-ΔPair Distribution Function Method**. *ChemPhysChem* **2022**, *23*, No. e202100857.
(40) Wakizaka, M.; Kumagai, S.; Wu, H.; Sonobe, T.; Iguchi, H.; Yoshida, T.; Yamashita, M.; Takaishi, S. Macro- and atomic-scale observations of a one-dimensional heterojunction in a nickel and palladium nanowire complex. *Nat. Commun.* **2022**, *13*, 1188.
(41) Aizu, K. Determination of the State Parameters and Formulation of Spontaneous Strain for Ferroelastics. *J. Phys. Soc. Jpn.* **1970**, *28*, 706−716.
(42) Carpenter, M. A.; Salje, E. H.; Graeme-Barber, A. Spontaneous strain as a determinant of thermodynamic properties for phase transitions in minerals. *Eur. J. Mineral.* **1998**, *10*, 621−691.
(43) Mian, M. R.; Iguchi, H.; Takaishi, S.; Murasugi, H.; Miyamoto, T.; Okamoto, H.; Tanaka, H.; Kuroda, S.-i.; Breedlove, B. K.; Yamashita, M. Multiple-Hydrogen-Bond Approach to Uncommon Pd(III) Oxidation State: A Pd-Br Chain with High Conductivity and Thermal Stability. *J. Am. Chem. Soc.* **2017**, *139*, 6562−6565.
(44) Yamashita, M.; Takaishi, S. Stabilization of Pd(iii) states in nano-wire coordination complexes. *Chem. Commun.* **2010**, *46*, 4438−4448.
(45) Xu, C.; Mao, J.; Guo, X.; Yan, S.; Chen, Y.; Lo, T. W.; Chen, C.; Lei, D.; Luo, X.; Hao, J.; Zheng, C.; Zhu, Y. Two-dimensional ferroelasticity in van der Waals β′-In2Se3. *Nat. Commun.* **2021**, *12*, 3665.
(46) Ju, C.; Yang, J.-C.; Luo, C.; Shafer, P.; Liu, H.-J.; Huang, Y.-L.; Kuo, H.-H.; Xue, F.; Luo, C.-W.; He, Q.; Yu, P.; Arenholz, E.; Chen, L.-Q.; Zhu, J.; Lu, X.; Chu, Y.-H. Anomalous Electronic Anisotropy Triggered by Ferroelastic Coupling in Multiferroic Heterostructures. *Adv. Mater.* **2016**, *28*, 876−883.
(47) Stinson, H. T.; Sternbach, A.; Najera, O.; Jing, R.; Mcleod, A. S.; Slusar, T. V.; Mueller, A.; Anderegg, L.; Kim, H. T.; Rozenberg, M.; Basov, D. N. Imaging the nanoscale phase separation in vanadium dioxide thin films at terahertz frequencies. *Nat. Commun.* **2018**, *9*, 3604.
(48) Agar, J. C.; Damodaran, A. R.; Okatan, M. B.; Kacher, J.; Gammer, C.; Vasudevan, R. K.; Pandya, S.; Dedon, L. R.; Mangalam, R. V. K.; Velarde, G. A.; Jesse, S.; Balke, N.; Minor, A. M.; Kalinin, S. V.; Martin, L. W. Highly mobile ferroelastic domain walls in compositionally graded ferroelectric thin films. *Nat. Mater.* **2016**, *15*, 549−556.
(49) Le Bail, A. Whole Powder Pattern Decomposition Methods and Applications: A Retrospection. *Powder Diffr.* **2005**, *20*, 316−326.

https://doi.org/10.1021/acs.inorgchem.2c02078
Inorg. Chem. 2022, 61, 14067−14074